Motion and Remelting of Dendrite Fragments during Directional Solidification of a Nickel-Base Superalloy

J.P. GU, C. BECKERMANN, and A.F. GIAMEI

The formation of spurious grains during the directional solidification of a Ni-base superalloy is studied by modeling the movement and remelting of dendrite fragments originating in channels inside the mush. Such channels exist because of thermosolutal convective instabilities during solidification and persist as freckle chains in the solidified material. The fragment model is linked to a phase equilibrium subroutine for multicomponent Ni-base superalloys, as well as to a previously developed solidification and convection code. A parametric study is performed to investigate the effects of initial fragment location and size on the fragment paths and survivability in the melt for one of the channels predicted in a typical directional solidification simulation. It is found that only a small window of initial conditions exists which leads to spurious grain formation. This window corresponds to medium-sized fragments originating near the mouth of the channel. Other fragments either remelt completely or sink into the channel. The need for an accurate fragment generation model is discussed.

I. INTRODUCTION

THE avoidance of grain defects is of critical importance in the directional solidification of single-crystal castings. Two types of defects commonly observed in Ni-base superalloy components are so-called freckle chains and isolated ''spurious'' grains, both of which can feature highly misoriented, equiaxed grains. Recent examples of such grain defects, including micrographs, can be found in the experimental work of Pollock and Murphy,[1] who noted that the onset of freckle formation occurs under the same conditions as for the spurious grains.

The formation of freckle chains or channel segregates due to thermosolutal convective instabilities is relatively well understood since the original work of Giamei and Kear.[2] In a companion article,[3] we presented a detailed solidification and melt convection model, coupled with a phase equilibrium subroutine for Ni-base superalloys, that allows for a realistic prediction of channel segregates in directional solidification of superalloys. The reader is referred to Reference 3 for a review of related work in this area. Figure 1 shows an example of model calculations for a convectively unstable case corresponding to the CMSX2 alloy. Noteworthy is the long, open channel in the mush, through which highly segregated liquid flows upward to feed a low-density plume, or finger, above the channel in the single-phase liquid region. In the solidified casting, the channels persist as regions of strong macrosegregation containing a chain of equiaxed grains.

The equiaxed grains inside the channels originate from separation of secondary or tertiary dendrite arms from the main trunks in the channels during solidification.[4,5,6] The separation is generally thought to occur at the joints (or ''necks'') between an arm and its trunk and is caused by localized remelting and coarsening. Hellawell[7] and others (references therein) have proposed mechanisms for the detachment process, but predictive models are not available. The separated dendrite fragments are subject to drag forces from the relatively strong melt flow in the channels, to their own weight, and to blocking by other dendrite arms. Sometimes, a fragment can rotate only slightly but stays otherwise fixed, leading to the presence of a minimally misoriented equiaxed grain in the channel (micrographs in Reference 1). The presence of highly misoriented grains in the channels indicates that some fragments undergo more extensive rotational and translational motion.

Experiments with transparent model alloys have shown that the low-density plumes associated with the channels sweep some of the dendrite fragments into the bulk liquid.[4–9] If the fragments survive in the melt above the mush, they can grow into equiaxed grains in front of the advancing columnar front and may even block it. Jackson *et al.*[4] were the first to show that such a scenario, involving fragments, can be responsible for a columnar-to-equiaxed transition. If only a few fragments are swept out and/or survive, they will block the columnar front only temporarily and eventually may be overgrown, leading to the presence of isolated spurious grains, depending on the orientation of the fragment relative to the parent grain. This mechanism for spurious grain formation in superalloy directional solidification was strongly suggested by the experiments of Pollock and Murphy.[1] It is opposed to other theories that rely on direct nucleation of equiaxed grains in the undercooled liquid in front of the columnar dendrite tips.[10–13]

The purpose of the present study is to investigate the possibility of fragments generated within channels to be advected by the bulk liquid and survive to form spurious grains. A model for the fragment movement and remelting is developed that pertains to realistic conditions involving a multicomponent Ni-base superalloy. This fragment model is linked to the directional solidification model for the prediction of channel segregates described in the companion article.[3] Parametric studies are performed for a typical directional solidification case to quantify the conditions necessary for fragments to cause spurious grain defects.

J.P. GU, Postdoctoral Researcher, and C. BECKERMANN, Professor, are with the Department of Mechanical Engineering, University of Iowa, Iowa City, IA 52242-1527. A.F. GIAMEI, Principal Scientist, is with the United Technologies Research Center, East Hartford, CT 06108.

Manuscript submitted October 28, 1996.

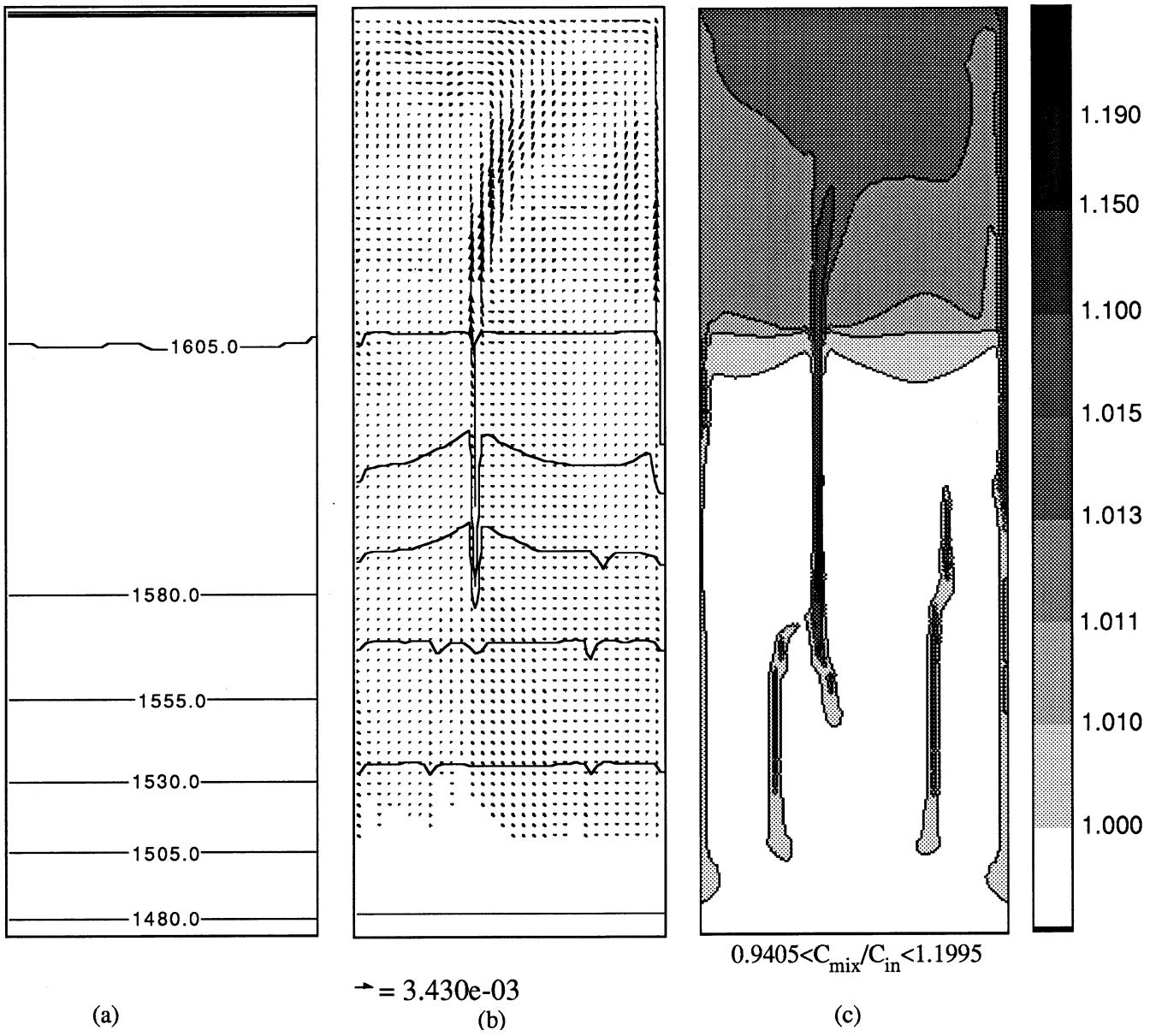

Fig. 1—The initial conditions for the calculation (from the directional solidification simulation of Case 4 at 5071 s in Ref. 3): (*a*) isotherms in Kelvin, (*b*) velocity vectors (in m/s) and solid fraction contours (in 20 pct increments) and (*c*) normalized mixture concentration pattern of Ti.

II. GOVERNING EQUATIONS

In modeling the motion and remelting of individual dendrite fragments, only the dilute limit of the fragment volume fraction tending to zero is considered. In other words, the effect of the fragments on the melt convection and solidification process modeled in Reference 3 is neglected. Of course, the changing melt velocity, temperature, and composition strongly influence the fate of the fragments, as modeled subsequently. A more comprehensive model of equiaxed solidification with melt convection that takes into account the motion of free crystals at any volume fraction has recently been presented.[14,15,16]

The translational motion of a dendrite fragment of velocity, $\mathbf{v}_s$, equivalent diameter, d, and density, ρ_s, can be described by Newton's law, *i.e.*,

$$\frac{d\mathbf{v}_s}{dt} = -\frac{3}{4}\frac{\rho_l}{\rho_s d}(\mathbf{v}_s - \mathbf{v}_l)|\mathbf{v}_s - \mathbf{v}_l|C_D + \left(1 - \frac{\rho_l}{\rho_s}\right)\mathbf{g} \quad [1]$$

where $\mathbf{v}_l$ and ρ_l are the velocity and density of the liquid (melt), respectively; C_D is a drag coefficient; $\mathbf{g}$ is the gravitational acceleration; and t is time. The first term on the right-hand side of Eq. [1] is the drag force exerted by the liquid, and the second is the buoyancy force. The liquid velocity, $\mathbf{v}_l$, is known from the directional solidification simulation of Reference 3. By assuming a spherical fragment shape, the drag coefficient can be calculated from[17]

$$C_D = \frac{24}{\mathrm{Re}}(1 + 0.15\mathrm{Re}^{0.687}) \quad [2]$$

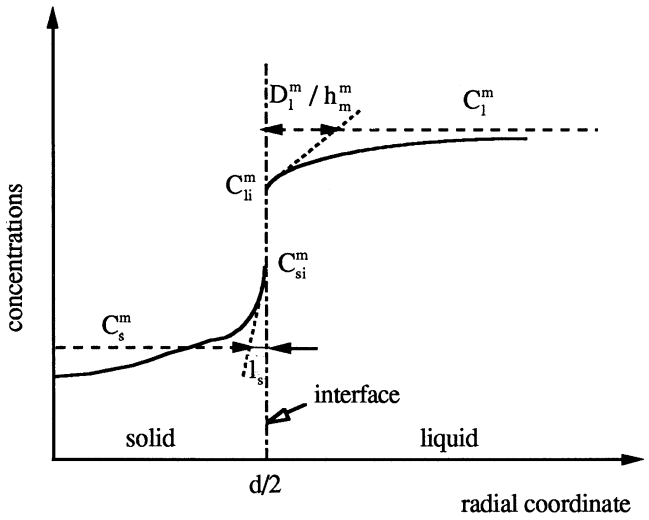

Fig. 2—Schematic illustration of the concentration profiles (for an element with a partition coefficient less than unity) and diffusion lengths for a melting fragment.

where Re is the Reynolds number based on the relative velocity between the dendrite fragment and the melt, *i.e.*,

$$\mathrm{Re} = \frac{|\mathbf{v}_s - \mathbf{v}_l|\rho_l d}{\mu} \qquad [3]$$

and μ is the melt viscosity. The second term on the right-hand side of Eq. [2] can be neglected, for $\mathrm{Re} < 0.2$. The solution of Eq. [1] requires an initial location, which is somewhere in the channel in the mush (Figure 1) as specified subsequently. The initial velocity is taken to be zero. At the end point of its path, the velocity of a surviving fragment is abruptly set to zero when the local volume fraction of solid (in the mush) predicted in the directional solidification simulation exceeds 0.01. At this point, the fragment is thought to be ''captured'' by the dendritic network. In reality, the solid fraction at which a fragment is captured will depend on the fragment size relative to the dendritic spacings and other factors, but the present choice is sufficiently realistic to determine an approximate end point of the path of a surviving fragment.

Remelting of the fragment in the bulk melt is a more complicated topic and requires careful consideration of the mass, species, and heat fluxes at the solid/liquid interface. As discussed in References 9, 18, and 19, there is a clear transition between thermally driven remelting at relatively high superheats and solutally driven *dissolution* at lower superheats. For example, for an alloy with vanishing solid solubility, remelting would always be thermally driven if the liquid temperature is above the melting point of the pure solvent. As can be seen in the left panel in Figure 1, in the present system the temperature of the melt above the mushy zone is relatively close to the liquidus temperature corresponding to the initial composition, and it can be verified that remelting in this melt is *solutally* driven. In fact, the fragment is small enough and the time scales are long enough that the fragment can safely be assumed to be in thermal equilibrium with the melt around it, and latent heat effects can be neglected. We will continue to call remelting what is actually modeled as a dissolution process.

Figure 2 shows a schematic illustration of the concentration profiles in the fragment and the surrounding melt during remelting (for an element with a partition coefficient less than unity). The *average* solute concentration of element m in the solid, C_s^m, changes due to phase change and back diffusion according to[20]

$$\rho_s V_s \frac{dC_s^m}{dt} = (C_{si}^m - C_s^m)\left(\rho_s \frac{dV_s}{dt} + \frac{\rho_s A_s D_s^m}{l_s}\right) \qquad [4]$$

where C_{si}^m is the solute concentration in the solid at the interface; $A_s = \pi d^2$ is the fragment surface area; $V_s = \pi d^3/6$ is the fragment volume; D_s^m is the diffusion coefficient of species m in the solid; and l_s is a solid diffusion length (Figure 2), which is defined as in other back-diffusion analyses.[20,21,22] The initial value of C_s^m is taken to be the one of the solid closest to the initial location of the fragment, as calculated in the directional solidification simulation. A balance of the species fluxes of element m at the solid/liquid interface gives the time rate of change of the fragment volume:[20]

$$(C_{li}^m - C_{si}^m)\,\rho_s \frac{dV_s}{dt} = \rho_l\, h_m^m\, A_s\,(C_{li}^m - C_l^m) + \frac{\rho_s A_s D_s^m}{l_s}(C_{si}^m - C_s^m) \qquad [5]$$

where C_l^m and C_{li}^m are the average and interfacial, respectively, solute concentrations in the liquid, and h_m^m is a convective mass transfer coefficient (of element m). The difference $(C_{li}^m - C_l^m)$ is the solutal undercooling or superheat in the liquid. The average liquid concentration, C_l^m, is known from the directional solidification simulation, while C_{li}^m is related to the temperature through the liquidus surface

Table I. Initial Fragment Locations and Sizes, and Summary of Results

x (m)	0.0189				0.0193				0.0197			
diameter (μm)												
y (m)	400	300	200	100	400	300	200	100	400	300	200	100
0.0963	⊗	●	○	○	⊗	●	○	○	⊗	●	○	○
0.0882	⊗	⊗	○	○	⊗	⊗	○	○	⊗	⊗	○	○
0.0821	⊗	⊗	⊗	∅	⊗	⊗	⊗	∅	⊗	⊗	⊗	∅
0.0740	⊗	⊗	⊗	⊗	⊗	⊗	⊗	⊗	⊗	⊗	⊗	⊗

●—Advected out of the channel, survives, and deposits on the mushy zone.
○—Advected out of the channel, but completely remelts.
⊗—Remains inside the channel and survives.
∅—Completely remelts within the channel.

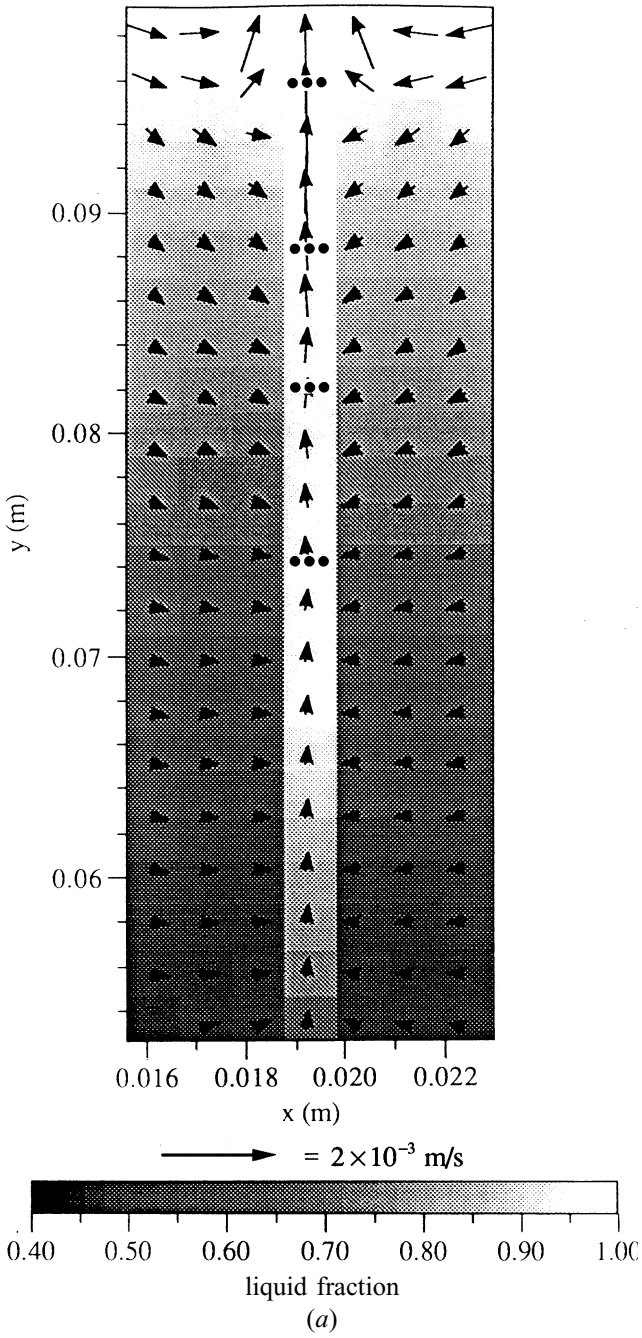

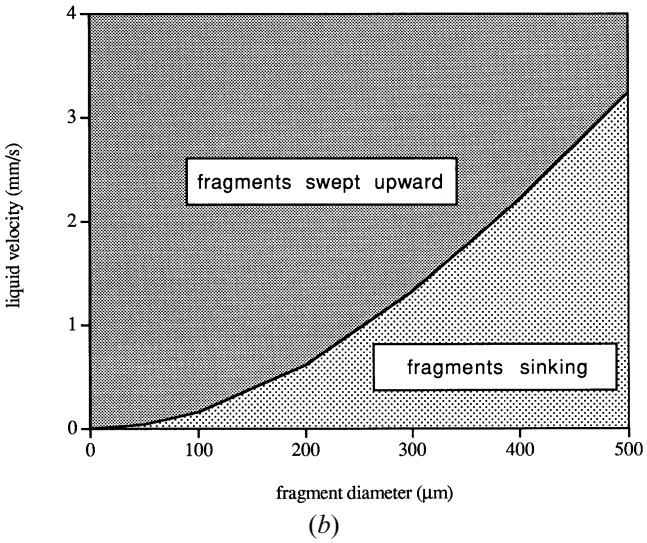

Fig. 3—(*a*) Initial fragment locations (black dots) in the center channel of Fig. 1. (*b*) Equilibrium liquid velocity at which a fragment of a given diameter is stationary due to a complete balance of drag and gravity forces.

and is obtained from phase equilibrium calculations, as subsequently shown. The definition of h_m^m is illustrated in Figure 2. In this study, h_m^m is calculated from a simple Sherwood number, Sh, correlation for spheres:[23]

$$\mathrm{Sh} = \frac{h_m^m d}{D_l^m} = 2.0 + 0.6\mathrm{Re}^{1/2}\,\mathrm{Sc}^{m1/2} \qquad [6]$$

where $\mathrm{Sc}^m = \mu/D_l^m/\rho_l$ is the Schmidt number, and D_l^m is the mass diffusivity in the liquid.

Equations [4] and [5] are generally valid and can, in theory, be solved for the evolutions of the fragment volume and concentrations. The principal difficulty lies in the specification of the interfacial concentration in the solid, C_{si}^m, and the solid diffusion length, l_s. For example, in the limit of no back diffusion, one would need to back up along the concentration profiles in the solid during remelting to obtain C_{si}^m.[24] This would require, in turn, storing (in computer memory) the concentration profiles at every point in the mushy zone as the solid forms—something that was not done. Alternatively, with the inclusion of back diffusion, C_{si}^m would be given by phase equilibrium. However, the diffusion length, l_s, cannot be based on the assumption of simple parabolic concentration profiles in the solid, as has been shown to be a good approximation in solidification analyses,[3,20–22] because during remelting the profiles are likely to contain local extrema and a very strong gradient near the interface.[24] Although this problem could be overcome by the choice of higher-order profile approximations, a more simple approach is taken in the present study. It is

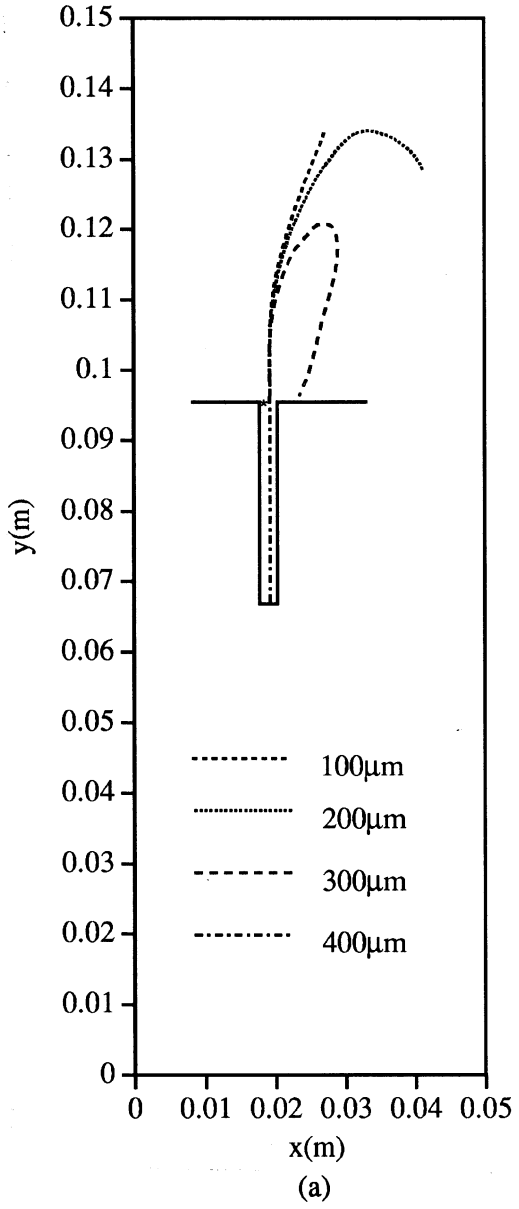

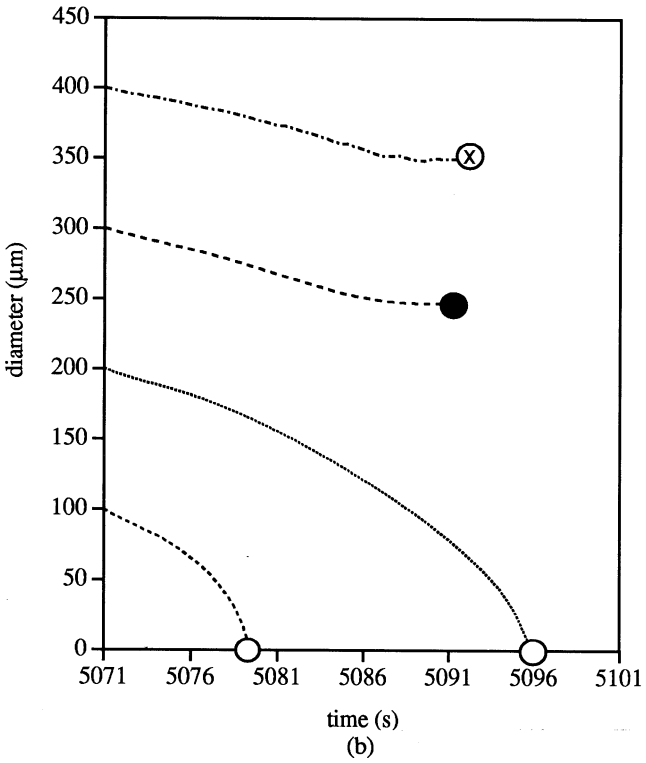

Fig. 4—Results for the initial fragment location at $x = 0.0192$ m and $y = 0.0963$ m and four different initial fragment diameters: (*a*) fragment paths and (*b*) evolution of fragment diameters.

assumed that the *average* solute concentrations in the fragment do not change during remelting, *i.e.*,

$$\frac{dC_s^m}{dt} = 0 \qquad [7]$$

Without resolidification, C_s^m would thus remain at the initial value where the fragment originated. Given the lack of knowledge of the exact concentration profiles in the initial fragment and other uncertainties in the model, the preceding approximation is still expected to give reasonable results for the average melting rate. Combining Eqs. [4] and [5], the back-diffusion term can now be eliminated to yield

$$(C_{li}^m - C_s^m)\,\rho_s \frac{dV_s}{dt} = \rho_l\, h_m^m\, A_s\, (C_{li}^m - C_l^m) \qquad [8]$$

Note the subtle difference in the left-hand sides of Eqs. [5] and [8], which originates from the preceding combination (C_s^m can still be different from C_{si}^m for interface equilibrium). Also note that all elements in the multicomponent alloy must satisfy Eq. [8] simultaneously and that C_{li}^m must be less than C_l^m (*i.e.*, the melt must be constitutionally superheated) for remelting to occur. The initial fragment volume needed to solve Eq. [8] is subsequently specified in a parametric study.

III. SOLUTION PROCEDURES

As detailed in Reference 3, phase equilibrium in the present simulations is calculated using the subroutine developed by Boettinger *et al.*[25] for Ni-base superalloys. In solving Eq. [8] for each solute, the equilibrium liquid concentrations at the interface, C_{li}^m, are linked to the known temperature, T, from the directional solidification simulation through the liquidus surface. Because all C_{li}^m cannot be calculated from the knowledge of temperature alone, an iterative procedure with a modified call to the phase

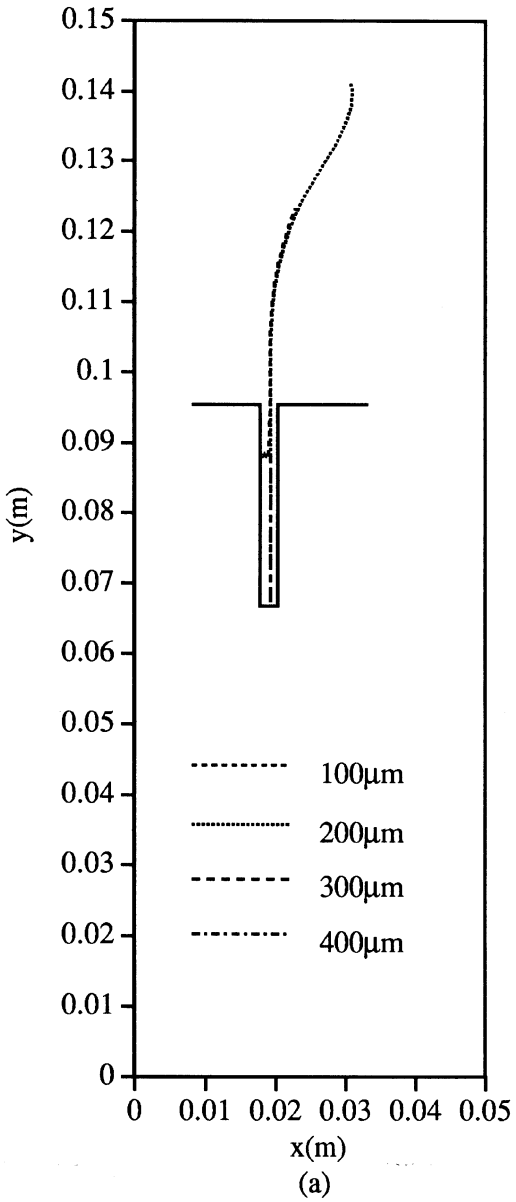

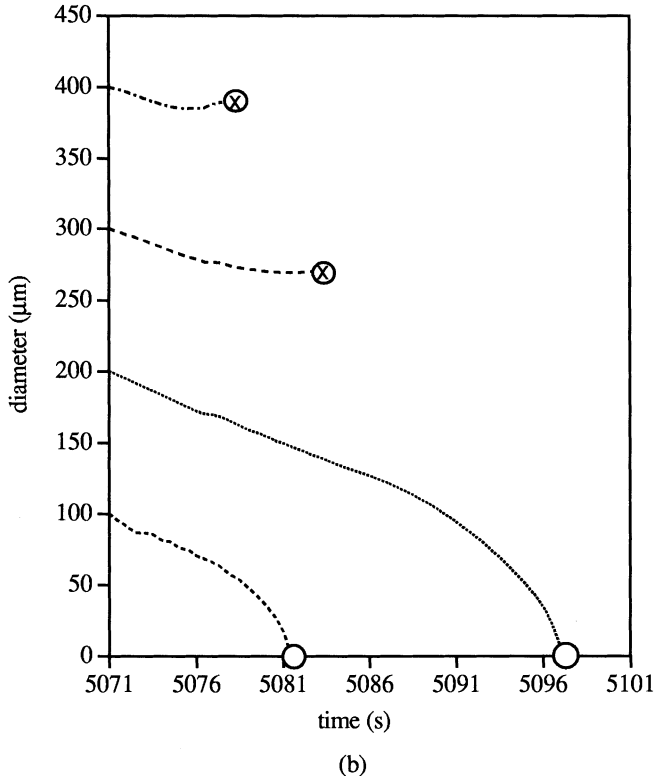

Fig. 5—Results for the initial fragment location at $x = 0.0192$ m and $y = 0.0882$ m and four different initial fragment diameters: (*a*) fragment paths and (*b*) evolution of fragment diameters.

equilibrium subroutine is required. The algorithm can be outlined as follows:

(a) guess all C_{li}^m;
(b) make the following call to the phase equilibrium subroutine:

$$T,\ C_{li}^m \text{ (for } n\text{-1 elements)} \Rightarrow C_{li}^m \text{ (for one element), others} \quad [9]$$

where n is the total number of solutes;
(c) solve Eq. [8] for one element to obtain dV_s/dt;
(d) solve Eq. [8] to update C_{li}^m for $(n - 1)$ elements; and
(e) go back to (b) until convergence.

The preceding procedure was found to converge quickly if some underrelaxation of the concentrations was used.

After updating the volume (or equivalent diameter) of the fragment at each time-step, the particle is moved according to the solution of Eq. [1]. All fragment calculations are performed simultaneously with the directional solidification simulation, so that the liquid velocity, temperature, and (average) concentrations continuously change in time and space. Equation [1] was discretized implicitly, whereas Eq. [8] was discretized explicitly. The results were found to be independent of the time-step. The liquid quantities are only available at the discrete grid points used in the directional solidification simulation[3] and were, thus, carefully interpolated to the location of the fragment. The calculations for a particular fragment were stopped when the fragment became stationary or when it completely remelted.

IV. CONDITIONS

The fragment motion and remelting calculations were performed in conjunction with the directional solidification simulation of Case 4 in Reference 3, because this simulation predicts a large open channel in the mush near the middle of the cavity (Figure 1). Case 4 simulates the solidification of the single-crystal, eight-element CMSX2 alloy (65.8Ni, 8.0Cr, 5.0Co, 1.0Ti, 6.0Ta, 5.6Al, 0.6Mo, and 8.0W, by wt pct) with a mean temperature gradient of 20 K/cm and a casting speed of 10 cm/h inside a 5 × 15 cm rectangular cavity. The primary dendrite arm spacing is 400

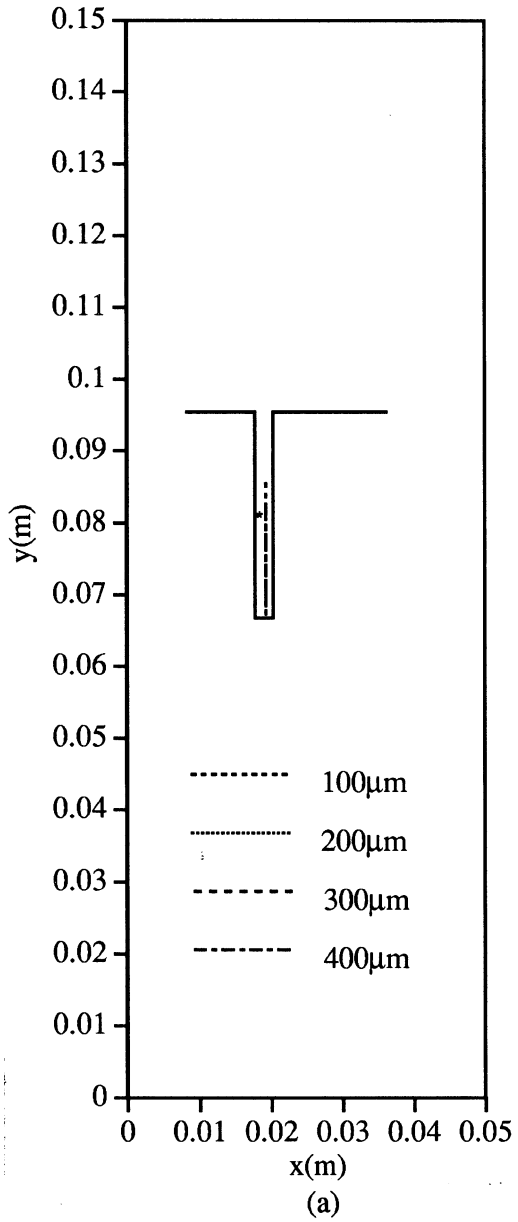

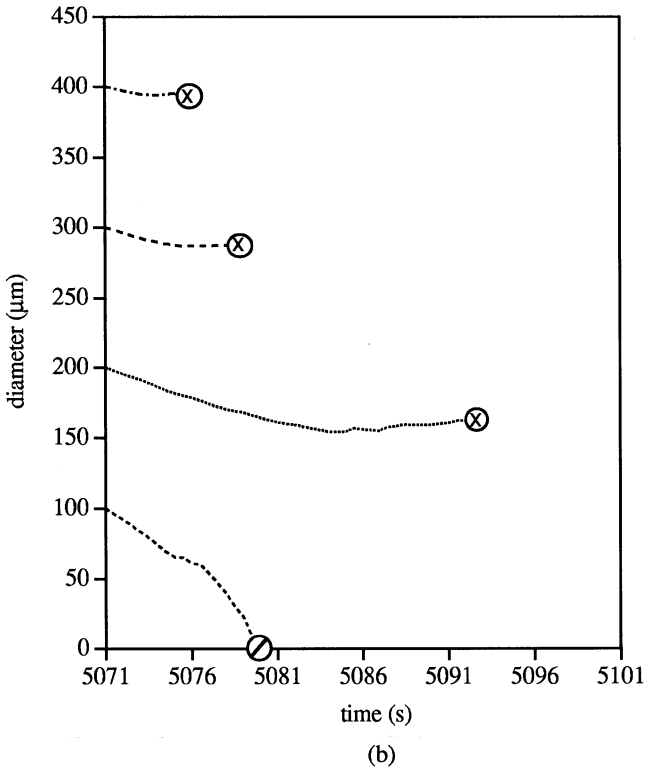

Fig. 6—Results for the initial fragment location at $x = 0.0192$ m and $y = 0.0821$ m and four different initial fragment diameters: (*a*) fragment paths and (*b*) evolution of fragment diameters.

μm.[3] The thermophysical properties and other conditions are the same as in Reference 3. As a first approximation, the density ratio, ρ_s/ρ_l, was taken to be 1.025, which was obtained through an extrapolation of available solid densities for Ni-base superalloys to the liquidus temperature.[26]

The fragment calculations were initiated at a time of 5071 seconds into the simulation of Case 4, for which the temperature, liquid velocity, solid fraction, and (Ti) species concentration fields are shown in Figure 1. Because of large initial and final transients due to a finite domain height, quasi-steady directional solidification conditions are never fully achieved in Case 4, and the fields continually evolve. Preliminary simulations revealed that at earlier times, when the middle channel is less developed, liquid velocities are too small to sweep fragments out of the channel into the bulk melt. The same is true at later times, when the flow above the channel strongly interacts with the top boundary. The present initial time (5071 seconds), as well as the casting parameters of Case 4, should therefore only be viewed as being representative of conditions where detached dendrite fragments can be swept into the bulk liquid, survive, and form spurious grains, as subsequently shown.

Since presently there is no theory available that allows for the prediction of dendrite detachment inside a channel, a parametric study was performed to investigate the effect of initial fragment location and size on the subsequent movement and remelting. The initial fragment locations are given in Table I and are illustrated in Figure 3(a). The origin of the coordinate system is in the lower-left corner of the domain (Figure 1). The 12 locations inside the channel correspond to four different heights with three points each, evenly distributed over the width (where the solid fraction is less than 0.01). At each location, four different initial fragment sizes (100-, 200-, 300-, and 400-μm diameter) were simulated. These sizes were thought to be representative of typical fragments observed in micrographs[1] and, as is subsequently shown, allow for a complete characterization of the fragment behavior in the present system. Certainly, a fragment much larger than the primary dendrite arm spacing would be unlikely to exist.

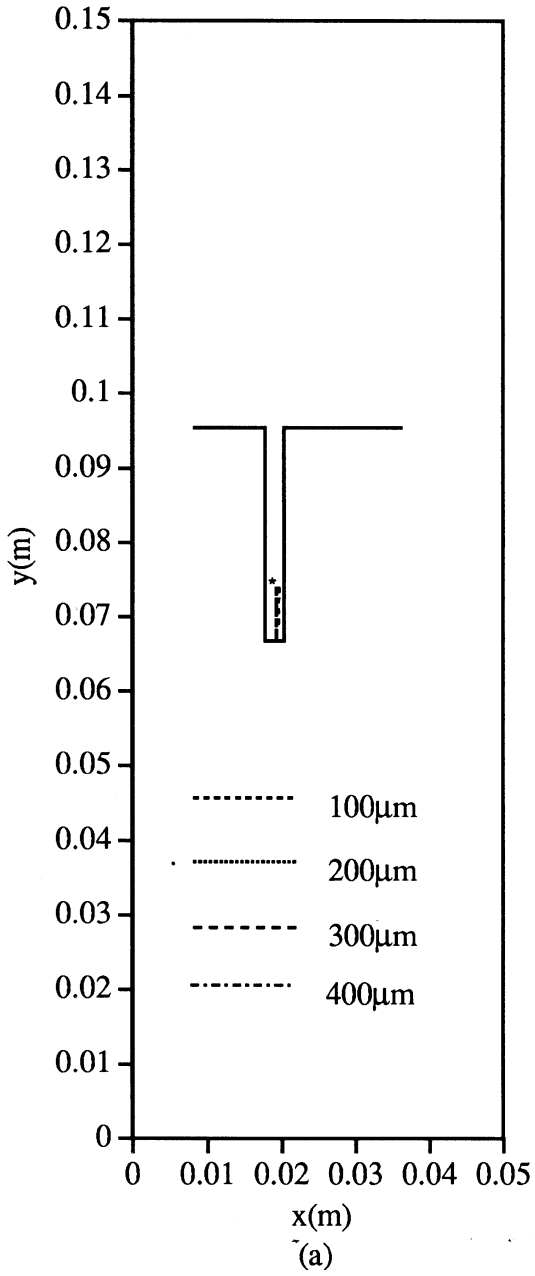

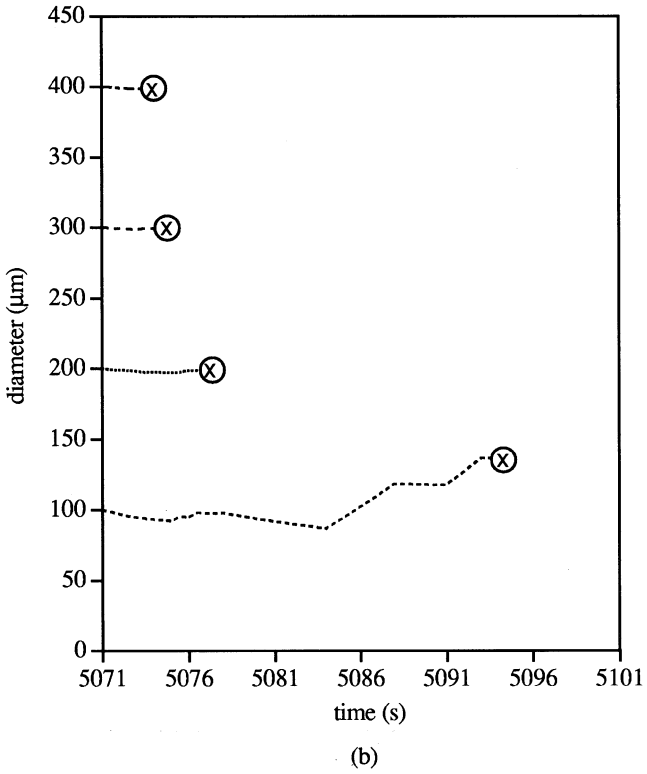

Fig. 7—Results for the initial fragment location at $x = 0.0192$ m and $y = 0.0740$ m and four different initial fragment diameters: (*a*) fragment paths and (*b*) evolution of fragment diameters.

The present choices of initial fragment diameters can also be understood by calculating from Eq. [1] the equilibrium liquid velocity at which a fragment of a certain diameter becomes stationary due to a complete balance of upwardly directed liquid drag and downwardly directed gravity forces. As illustrated in Figure 3(b), for the range of liquid velocities encountered in the channel of the present directional solidification simulation (Figure 3(a)), a fragment would need to be smaller than about 400 μm to be swept out into the bulk liquid. It should be kept in mind that this range of velocities is unique to the conditions of Case 4 in Reference 3, and other alloys and casting conditions will produce different velocities. As discussed in the companion article, the predicted plume velocities are thought to be realistic for the limited buoyancy forces and mush permeabilities present in Case 4.

V. RESULTS AND DISCUSSION

The results for each of the four initial heights are shown in Figures 4 through 7. The paths of the fragments were found to be relatively insensitive to the horizontal location in the channel, and only the results for the middle location are shown in the figures. The fate of all simulated fragments is summarized in Table I.

Figure 4(a) shows the paths of each of the four initial fragment sizes for a launching point near the mouth of the channel. The three smaller fragments are advected vertically upward out of the channel, whereas the 400 μm fragment sinks to the bottom of the channel (until the solid fraction becomes greater than 0.01). The paths of the three smaller fragments start to differ once the liquid velocities become smaller in the upper part of the liquid region (Fig-

ure 1) and the size differences start to dominate. The corresponding time evolutions of the fragment diameters are shown in Figure 4(b). It can be seen that the 100 and 200 μm fragments survive about 9 and 25 s, respectively. Since the lengths of their paths are similar, it is clear that the smaller one moves at a much higher velocity. This can be expected from Eq. [1], because the relative velocity, $|\mathbf{v}_l - \mathbf{v}_s|$, decreases with decreasing diameter, d. On the other hand, the diameter of the 300 μm fragment decreases much less (although the melting rates are about the same), and this fragment eventually sinks back down and hits the top of the mushy zone not too far away from the mouth of the channel. Such surviving fragments will then continue to grow in the imposed temperature gradient. They can either be overgrown by the advancing columnar dendrites or propagate at the expense of the parent crystal, depending on both crystal orientations and growth direction. In any case, the surviving fragments are a source of spurious grains in directional solidification. The coincidence between freckle formation and the presence of spurious grains in Ni-base superalloy solidification has been noted by Pollock and Murphy,[1] who show some micrographs of such grains embedded in the otherwise single-crystal structure. If many fragments survive, they can completely block the advancing columnar front and cause a columnar-to-equiaxed transition, as also shown in Reference 1. Although the largest (400 μm) fragment sinks directly into the channel, its diameter decreases too, indicating that the upward flowing melt in the channel is constitutionally superheated. Only near the bottom, the fragment starts to grow again. The presence of (equiaxed) grains inside freckles has already been discussed in Section I.

The results for an initial fragment location 8.1 mm further down in the channel are shown in Figure 5. The main difference to the previous figure is that only the 100 and 200 μm fragments are advected out of the channel, while both large ones sink into it. This can be explained by the lower liquid velocities further down in the channel. Both of the smaller fragments remelt completely. Indeed, additional simulations for this initial location did not yield a fragment size that results in a surviving fragment outside of the channel and, hence, any spurious grains.

Figure 6 shows results for an initial fragment location at about midheight in the open channel. None of the fragments is advected out of the channel, although the smallest one (100 μm) moves slowly upward a small distance until it completely remelts. The larger three fragments sink into the channel and survive. In fact, they remelt only slightly (Figure 6(b)). Note that the sink time is, as expected, much longer for the 200 μm fragment than for the 300 and 400 μm fragments.

Finally, Figure 7 indicates that, if free dendrite fragments are generated in the lower half of the open channel, they will all sink into it and survive. The diameters of the three larger ones stay about constant, while the smallest fragment actually grows before becoming stationary. This far down into the channel, the melt flow is too weak to advect fragments against gravity, and the melt is very close to liquidus conditions.

VI. CONCLUSIONS

The motion and remelting of free fragments originating in channels inside the mushy zone during directional solidification of a single-crystal Ni-base superalloy has been investigated for several initial fragment sizes and locations inside a typical channel. The parametric study indicates that there exists only a relatively small window of initial conditions that result in a fragment being advected out of the channel, surviving, and ultimately forming an isolated spurious grain. In the present system, this window corresponds to medium-sized fragments (around 300 μm) originating near the mouth of the channel. If the fragments are too small, they may be advected out of the channel but remelt completely in the melt above the mushy zone. If the fragments are too large or originate too low in the channel, they remain inside the channel, where most survive and form the equiaxed grains usually observed in freckle defects.

The present study corroborates the experimental findings of Pollock and Murphy[1] regarding the simultaneous occurrence of freckle defects and spurious grains, linking their origin to fragmentation of dendrites. However, the model does not allow for the prediction of the exact final location of spurious grains in superalloy castings. This is due to the fact that no relation is available to calculate the exact location, time, and frequency of fragment generation in a channel. Even if such a relation were available, it is unlikely that the initial fragment size would be known with much accuracy. The present results show that the fragment survivability and final location are quite sensitive to the initial conditions.

Although the calculations provide some insight into fragment motion and remelting, they were only performed for *typical* casting conditions and one alloy composition. The fragment behavior will be different for other imposed temperature gradients, casting speeds, or alloy compositions, making it difficult to derive general criteria for spurious grain formation. However, linking the fragment calculations to comprehensive solidification simulations, as was done here, provides some predictive capabilities.

ACKNOWLEDGMENTS

This work was supported in part by the Advanced Research Project Agency, under the Micromodeling program of the Investment Casting Cooperative Arrangement (ICCA) through a subcontract to Howmet Corporation (Dr. Boyd Mueller, technical contact), and by the National Science Foundation, under Grant No. CTS-9501389. The authors thank W.J. Boettinger and U.R Kattner, NIST, for their help with the phase equilibrium subroutine and other fruitful discussions.

REFERENCES

1. T.M. Pollock and W.H. Murphy: *Metall. Mater. Trans. A*, 1996, vol. 27A, pp. 1081-94.
2. A.F. Giamei and B.H. Kear: *Metall. Trans.*, 1970, vol. 1, pp. 2185-92.
3. M.C. Schneider, J.P. Gu, C. Beckermann, W.J. Boettinger, and U.R. Kattner: *Metall. Mater. Trans. A*, 1997, vol. 28A, pp. 1517-31.
4. K.A. Jackson, J.D. Hunt, D.R. Uhlmann, and T.P. Senard: *Trans. AIME*, 1966, vol. 236, pp. 149-58.
5. S.M. Copley, A.F. Giamei, S.M. Johnson, and M.F. Hornbecker: *Metall. Trans.*, 1970, vol. 1, pp. 2193-2204.
6. A. Hellawell, J.R. Sarazin, and R.S. Steube: *Phil. Trans. R. Soc. London A*, 1993, vol. 345, pp. 507-44.
7. A. Hellawell: in *Modeling of Casting, Welding and Advanced*

Solidification Process VII, M. Cross and J. Campbell, eds., TMS, Warrendale, PA, 1995, pp. 565-76.
8. R.S. Steube and A. Hellawell: *Int. Video J. Eng. Res.*, 1993, vol. 3, pp. 1-16.
9. G. Hansen, A. Hellawell, S.Z. Lu, and R.S. Steube: *Metall. Mater. Trans. A*, 1996, vol. 27A, pp. 569-81.
10. W.C. Winegard and B. Chalmers: *Trans. ASM*, 1954, vol. 46, pp. 1214-22.
11. J.D. Hunt: *Mater. Sci. Eng.*, 1984, vol. 65, pp. 75-83.
12. C.Y. Wang and C. Beckermann: *Metall. Mater. Trans. A*, 1994, vol. 25A, pp. 1081-93.
13. Ch.-A. Gandin and M. Rappaz: *Acta Metall. Mater.*, 1994, vol. 42, pp. 2233-46.
14. C.Y. Wang and C. Beckermann: *Metall. Mater. Trans. A*, 1996, vol. 27A, pp. 2754-64.
15. C.Y. Wang and C. Beckermann: *Metall. Mater. Trans. A*, 1996, vol. 27A, pp. 2765-83.
16. C. Beckermann and C.Y. Wang: *Metall. Mater. Trans. A*, 1996, vol. 27A, pp. 2784-95.
17. A.R. Khan and J.F. Richardson: *Chem. Eng. Comm.*, 1987, vol. 62, pp. 135-50.
18. R.C. Kerr: *J. Fluid Mech.*, 1994, vol. 280, pp. 255-85.
19. A.W. Woods: *J. Fluid Mech.*, 1992, vol. 239, pp. 429-48.
20. C.Y. Wang and C. Beckermann: *Metall. Trans. A*, 1993, vol. 24A, pp. 2787-2802.
21. C.Y. Wang and C. Beckermann: *Mater. Sci. Eng.*, 1993, vol. A171, pp. 199-211.
22. M.C. Schneider and C. Beckermann: *Metall. Mater. Trans. A*, 1995, vol. 26A, pp. 2373-88.
23. W. Ranz and W. Marshall: *Chem Eng. Progr.*, 1952, vol. 48, p. 144.
24. M. Rappaz and V. Voller: *Metall. Trans. A*, 1990, vol. 21A, pp. 749-53.
25. W.J. Boettinger, U.R. Kattner, S.R. Coriell, Y.A. Chang, and B.A. Mueller: in *Modeling of Casting, Welding and Advanced Solidification Process VII*, M. Cross and J. Campbell, eds., TMS, Warrendale, PA, 1995, pp. 91-98.
26. B. Mueller: Howmet Corporation, Whitehall, MI, personal communication, 1995.